An experimental LPV/H ∞ direct yaw moment control for vehicle handling

Isabella P Manzini, Maud Geoffriault, Marcelo Menezes Morato, Olivier Sename

▶ **To cite this version:**

Isabella P Manzini, Maud Geoffriault, Marcelo Menezes Morato, Olivier Sename. An experimental LPV/H ∞ direct yaw moment control for vehicle handling. ROCOND 2025 - 11th IFAC Symposium on Robust Control Design, Jul 2025, Porto, Portugal. ⟨hal-05070908⟩

HAL Id: hal-05070908

https://hal.science/hal-05070908v1

Submitted on 16 May 2025

HAL is a multi-disciplinary open access archive for the deposit and dissemination of scientific research documents, whether they are published or not. The documents may come from teaching and research institutions in France or abroad, or from public or private research centers.

L'archive ouverte pluridisciplinaire **HAL**, est destinée au dépôt et à la diffusion de documents scientifiques de niveau recherche, publiés ou non, émanant des établissements d'enseignement et de recherche français ou étrangers, des laboratoires publics ou privés.

HAL Authorization

An experimental LPV/$\mathcal{H}_\infty$ direct yaw moment control for vehicle handling

Isabella P. Manzini [*] **Maud Geoffriault** [**]
Marcelo M. Morato [*,***] **Olivier Sename** [***]

[*] *Dept. de Eng. de Automação e Sistemas (*EAS*), Univ. Fed. de Santa Catarina (*UFSC*), Florianópolis-SC, Brazil.*
[**] *Ampère Software & Techonology, Technocentre, 1 avenue du Golf, 78280 Guyancourt*
[***] *Univ. Grenoble Alpes, CNRS, Grenoble INP*$^\top$*, GIPSA-lab, 38000 Grenoble, France.* $\top$*Institute of Engineering, Univ. Grenoble Alpes. (isabella.p.manzini@gmail.com)*

Abstract: In this work, we propose and experimentally validate a novel $\mathcal{H}_\infty$ scheme for direct yaw moment control of modern vehicles. In particular, the proposed scheme seeks to enhance the robustness of a real (state-of-practice) PIDs. To this end, we tune the robust controller using the so-called "bicycle model", accounting for a Linear Parameter Varying (LPV) reference model with consistent weights w.r.t. vehicle handling performance objectives. Accordingly, we present high-fidelity numerical validation results, along with real experimental vehicle tests under critical driving conditions in realistic city and mountain track circuits. Our findings confirm that the proposed LPV/$\mathcal{H}_\infty$ scheme indeed improves overall vehicle handling and driving stability.

Keywords: $\mathcal{H}_\infty$ control, Experimental validation, Vehicle Lateral Stability.

1. INTRODUCTION

In the scope of dynamic control of road vehicles, it is well-known that appropriately managing the lateral motion is an essential topic to ensure safety, proper handling, and an optimised driving experience (Kiencke et al., 2006). Accordingly, several prominent control systems have been proposed over the last years, with special focus on stability, cf. (Doumiati et al., 2010b; Aripin et al., 2014; Nahidi et al., 2017; Morato et al., 2019; Lenzo et al., 2020; Medero et al., 2022; Morato et al., 2022; Hachem et al., 2023).

The aforementioned works indeed highlight that handling lateral performances is especially important during high-speed driving and emergency manoeuvrers. In particular, road vehicles often face challenging conditions, such as driving over wet or icy surfaces - where appropriate managing lateral dynamics becomes crucial for maintaining stability and preventing loss of grip or sliding, as illustrates Fig. 1. However, to tune a consistent lateral control scheme is a complex (multi-objective) task, given that vehicle parameters (tire stiffness, mass, etc) are inherently time-varying - due to the car's lifespan and unpredictable natural (road) conditions. To this end, as discussed in the recent tutorial paper (Sename et al., 2024), robust control methods present a viable solution to ensure consistency and stability under all typical driving situations.

Nevertheless, when we investigate the industrial state-of-practice of lateral vehicle control, we observe that typically, (adaptive) PID controllers are tuned via extensive testing across various conditions, cf. (Kissai, 2019). Then, during the implementation, large look-up tables are used to adjust the PID gains according to the different driving situations. Due to the well-known limitations of PID schemes - particularly, possible lack of robustness -, in this work, we propose a novel $\mathcal{H}_\infty$ scheme to enhance tracking performance under uncertainties and disturbances, including a Linear Parameter Varying (LPV) reference model. Our main **contributions** are the following:

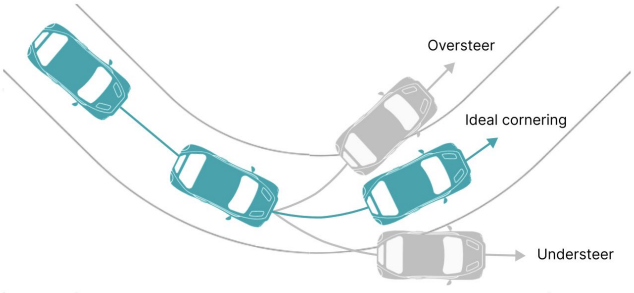

Fig. 1. Vehicle performing cornering motion.

(1) We propose a $\mathcal{H}_\infty$ scheme for the direct yaw moment control, which incorporates an LPV reference model in its synthesis.
(2) Several realistic numerical simulations are conducted to test and evaluate the proposed scheme.
(3) We provide real experimental validation results, in city and mountain-alike driving circuits, debating the advantages of the $\mathcal{H}_\infty$ scheme w.r.t. industrial PIDs used in real cars.

The rest of this paper is organised as follows: first, we recap topics on vehicle motion control (Sec. 2); the used bicycle model is detailed in Sec. 3; subsequently, the proposed LPV/$\mathcal{H}_\infty$ scheme is detailed in Sec. 4; numerical and

experimental results are presented and discussed in Sec. 5, which is followed by a brief conclusion (Sec. 6).

2. VEHICLE MOTION CONTROL

Next, we recap the main elements of industrial (state-of-practice) lateral vehicle control schemes, as detailed in (Kissai, 2019) - herein denoted "Vehicle Motion Control" (VMC). The goal of VMC is to coordinate and optimise differential braking of road cars. To this end, an Electronic Stability Control (ECU) is used to apply differential braking between right and left wheels, along with a rear wheel steering system. VMC loops are set closed-loop, so the vehicle follows a yaw rate reference trajectory and optimises the overall behaviour both at high (when stability is critical) and low speeds (when handling is critical).

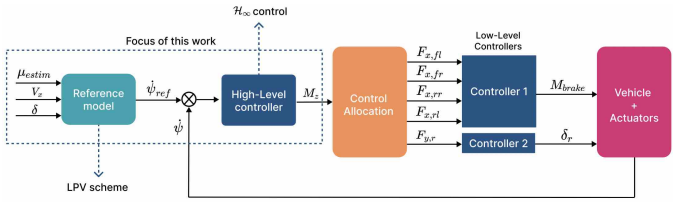

Fig. 2. Vehicle Motion Control Scheme.

A general schematic of VMC is presented in Fig. 2. The main elements are:

- The **reference model**, which defines the car's overall behavior based on driver inputs, including the driver's steering angle δ, vehicle longitudinal speed $V_x(t)$, and an estimated road friction coefficient μ. Based on these variables, the reference model generates a yaw rate reference signal $\dot{\psi}_{ref}$, which serves as the input for the "high-level controller". In this work, we propose an LPV reference model to generate and adequate set-points $\dot{\psi}_{ref}$ w.r.t. each operational condition.
- The **high-level controller** - typically implemented using a look-up table PID scheme, as previously detailed -, based on the yaw rate tracking error $(\dot{\psi}_{ref} - \dot{\psi})$ generates a yaw moment control input M_z, which is passed to a "control allocation" module. We note that this controller is the focal point of this work - for which we develop a $\mathcal{H}_\infty$ scheme.
- Accordingly, the **control allocation** module takes into account chassis limitations (constraints) and employs optimisation techniques in order to achieve optimal force distribution across the four wheels. This module is also responsible for adjusting the control law to the varying road adhesion conditions to improve both comfort and vehicle stability. The result are five outputs: four forces $F_{x,ij}$ that represent the traction distribution at each wheel, where $i = \{\text{front, rear}\}$ and $j = \{\text{left, right}\}$, corresponding to a 4-Wheel-Drive (4WD) vehicle configuration; and the lateral force generated by the rear steer angle $F_{y,r}$.
- Finally, the **low-level control** generates a braking moment M_{brake} and a rear steering angle δ_r, which are both directly sent to the **actuators** for execution.

3. VEHICLE DYNAMICS

For our control synthesis procedure, we consider a well-established (linearised) "bicycle" model, as briefly detailed next - complete discussions are available, e.g., in (Zhao et al., 2006; Sename et al., 2013). In practice, the considered model is quite practical since the car's lateral and yaw dynamics are simplified under reasonable (motion-related) assumptions. Specifically, the motion of the left and right wheels of the car (on the front and rear axles) are analysed as a single wheel along the centerline axis. Additionally, we consider that no braking is applied to any of the wheels, and the center of gravity (CoG) of the car remains fixed despite variations in the chassis' mass. Accordingly, the inputs of the bicycle model are the steering angle applied to the front wheels, denoted δ_f (which is the driver's steering δ summed to the corrective steer-by-wire command), and the yaw moment applied to the CoG, denoted M_z. The corresponding outputs are the vehicle sideslip angle β and its yaw rate $\dot{\psi}$.

Considering that the tires exhibit linear behaviors, that the vehicle motion is under a constant longitudinal velocity V_x, and neglecting pitch and roll dynamics, we account for the following LTI model given in state-space format:

$$\begin{bmatrix}\dot{\beta}(t)\\ \ddot{\psi}(t)\end{bmatrix} = \begin{bmatrix} -\frac{C_f+C_r}{mV_x} & -\frac{C_fL_f-C_rL_r}{mV_x^2} - 1 \\ -\frac{C_fL_f-C_rL_r}{I_z} & -\frac{C_fL_f^2+C_rL_r^2}{I_zV_x}\end{bmatrix}\begin{bmatrix}\beta(t)\\ \dot{\psi}(t)\end{bmatrix} + \begin{bmatrix}\frac{C_f}{MV_x}\\ \frac{L_fC_f}{I_z}\end{bmatrix}\delta_f(t) + \begin{bmatrix}0\\ \frac{1}{I_z}\end{bmatrix}M_z(t), \quad (1)$$

with corresponding parameters described in Table 1.

Symbol	Parameter description
m	Vehicle mass (kg)
V_x	Longitudinal velocity (ms)
L_f	Distance from front axle to CoG (m)
L_r	Distance from rear axle to CoG (m)
I_z	Moment of inertia (kgm^2)
C_f	Front tire cornering stiffness (N)
C_r	Rear tire cornering stiffness (N)

Table 1. Vehicle model parameters.

4. PROPOSED LPV/$\mathcal{H}_\infty$ FRAMEWORK

The goal of this paper is to experimentally validate a robust LPV/$\mathcal{H}_\infty$ solution to the **reference model** and the **high-level controller** blocks in the scheme shown in Fig. 2. In particular, we propose, respectively, an adaptive, LPV reference model and a dynamic output-feedback $\mathcal{H}_\infty$ controller. These two structures are detailed next.

4.1 LPV reference model

A fundamental aspect of the proposed robust lateral scheme for direct yaw motion control is the inclusion of a reference model, as depicted in Fig. 2. In particular, we use an LPV state-space realisation of the following format:

$$\begin{pmatrix}\dot{x}_{ref}(t)\\ \dot{\psi}_{ref}(t)\end{pmatrix} = \left[\begin{array}{c|c} A_r(\rho(t)) & B_r(\rho(t)) \\ \hline C_r(\rho(t)) & D_r(\rho(t))\end{array}\right]\begin{pmatrix}x_{ref}(t)\\ \delta(t)\end{pmatrix}. \quad (2)$$

The LPV reference model in Eq. (2), thus, generates a yaw rate signal $\dot{\psi}_{ref}(t)$ for different steering angle inputs $\delta(t)$ - provided by the car's pilot when driving. Furthermore, the LPV scheme is scheduled by the time-varying parameters $\rho(t) = \text{col}\,(V_x(t), \mu_{estim}(t))$, being μ_{estim} an estimate for the road friction coefficient μ. Matrices $A_r(\cdot)$, ..., $D_r(\cdot)$ in (2) are of appropriate dimension.

The output of Eq. (2), i.e., the yaw rate signal $\dot{\psi}_{ref}(t)$, is passed to the $\mathcal{H}_\infty$ generalised plant as the reference signal $r(t)$. We stress that, in practice, incorporating such LPV reference model was crucial for the success of our $\mathcal{H}_\infty$ controller. During experimental testing, the $\mathcal{H}_\infty$ controller without the LPV reference model was not able to adapt itself to harsh road friction and longitudinal velocity variations, and thus exhibited an overly aggressive behaviour, which could be unsatisfactory in certain driving situations.

4.2 Dynamic output-feedback $\mathcal{H}_\infty$ controller

Taking into account the LPV reference model in Eq. (2), our lateral control scheme is tuned as follows: we consider an optimisation (synthesis) problem that seeks to minimise the $\mathcal{H}_\infty$ norm of the closed-loop transfer function from the system disturbances ω to controlled outputs z. That is, our dynamic $\mathcal{H}_\infty$ controller $K(s)$ is given by the solution of:

$$\min_{\{\gamma_\infty, A, \ldots, C_2\}} \|T_{z\omega}\|_\infty \leq \gamma_\infty, \tag{3}$$

$$\text{s.t.:} \left\{ \begin{bmatrix} \dot{x} \\ \hline z \\ y \end{bmatrix} = \left[\begin{array}{c|cc} A & B_1 & B_2 \\ \hline C_1 & D_{11} & D_{12} \\ C_2 & 0 & 0 \end{array}\right] \begin{bmatrix} x \\ w \\ u \end{bmatrix} \right. , \gamma_\infty > 0.$$

In (3), $\omega = [\dot{\psi}_{ref}, d_i]^T$ represents the vehicle disturbances, being d_i and input load signal, $u = M_z$ the control input (yaw moment), $y = \dot{\psi}$ the measured output variables, $z = [z_1, z_2]^T$ the weighted controlled outputs, and x the system state variables, considering Eq. (1).

Accordingly, as done in standard robust control design practice (Sename et al., 2013), we use appropriate performance templates to define the desired system behaviour criteria. In particular, we take into account the following performance goals: reference tracking accuracy, disturbance rejection, and control input noise attenuation. These criteria are translated as weighting functions, denoted henceforth $W_e(s)$, $W_d(s)$, and $W_u(s)$, respectively. Each weighting function is shaped to penalise the deviations of the involved variables w.r.t. a desired performance.

The shape of the tracking-related weight is defined as:

$$W_e(s) = \left(\frac{s + \omega_s \epsilon_0}{\frac{s}{M_s} + \omega_s} \right)^{-1}, \tag{4}$$

where ω_S is the cut-off frequency of the high pass filter, ϵ_0 is the attenuation level for low frequencies ($f < \omega_S$). As standard, we use M_S to denote the maximum magnitude peak of the closed-loop sensibility function $S(s)$ defined as:

$$S(s) = \frac{1}{1 + K(s)G(s)}, \tag{5}$$

Similarly, the shape of $W_u(s)$, related to the measurement effect on the control input, is defined as:

$$W_u(s) = \left(\frac{\epsilon_1 + \omega_u}{s + \frac{\omega_u}{M_u}} \right)^{-1}, \tag{6}$$

where ω_u is the cut-off frequency of the low pass filter, ϵ_1 is the attenuation level for high frequencies ($f > \omega_u$) and M_u is the actuator saturation.

Notwithstanding, the weighting function $W_d(s)$, related to the rejection of the input disturbance d_i, is taken simply as a static gain - in order to upper bound the effect of disturbances.

The parameter values for each transfer function ($W_e(s)$, $W_d(s)$ and $W_u(s)$) are industry-confidential, being optimised through frequency-domain analysis. Adequate parameter were selected in order to ensure a balanced trade-off between disturbance rejection, robustness, response time, and noise attenuation.

In Fig. 3, we provide an example of a vehicle-based sensitivity function $S(s)$ along with a corresponding template $W_e(s)$. In this figure, the weight template is depicted as upper bound limits, defined by the inverse of the weighting function $W_e^{-1}(s)$. By analysing Fig. 3, we can indeed infer that the steady-state tracking error is small (and output disturbance rejection) - notice that $|S(j\omega)| = -38$ dB as ω approaches 0 rad/s, representing low-frequency attenuation. Additionally, the maximum peak criterion (module margin) is also satisfied, i.e. $\|S\|_\infty < M_S$.

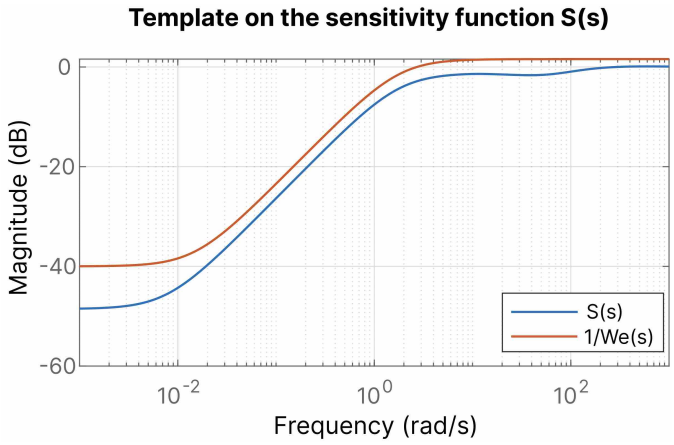

Fig. 3. Closed-loop sensitivity $S(s)$ and template $W_e^{-1}(s)$).

For further clarity, Fig. 4 shows a complete control synthesis block diagram of proposed $\mathcal{H}_\infty$ scheme. In this scheme, we indicate the main components of the generalized synthesis plant $P(s)$: the weighting functions $W_d(s)$, $W_e(s)$, and $W_u(s)$, as well as the plant model $G(s)$ - i.e. the bicycle model from Eq. (1) - and the proposed dynamic output-feedback controller $K(s)$ - i.e. the $\mathcal{H}_\infty$ scheme. The inputs $P(s)$ are defined as the reference signal $r(t)$, a generic input disturbance $d_i(t)$ represents a generic load disturbance variable (to account for, e.g. wind, model parameter variations along time, etc) and the control input $u(t)$. The outputs include the weighted tracking error $z_1(t)$, the tracking error ϵ and the weighted control effort $z_2(t)$.

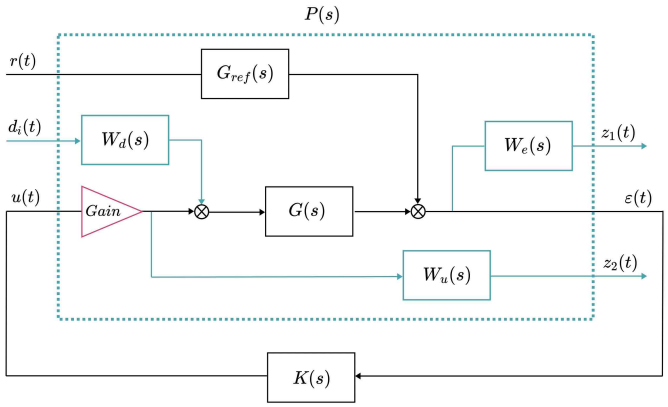

Fig. 4. $\mathcal{H}_\infty$ scheme with mixed weighting functions.

4.3 Control parametrization

In addition to the detailed developments, during the initial experimental essays related to this work, a thorough frequency-domain analysis w.r.t. (1) revealed that to develop a controller based on the yaw moment variable M_z as the control input presents a particular practical challenge. Due to the notably low direct gain from M_z to the controlled variable $\dot{\psi}$ at low frequencies, which subsequently impacts the overall open-loop gain. Thus, controlling the yaw rate using the yaw moment would require a very high gain at low frequency w.r.t. the error template $W_e(s)$ and a very low gain w.r.t. $W_u(s)$. Attempts to develop control strategies directly using M_z led to ineffective performance, characterised by non-robust behaviours.

In order to address this issue, an alternative solution was employed: the control synthesis is done using the front (additional) steering angle (δ_f) as input, which is then translated to a yaw moment input. Such an approach has consistency with results already registered in the literature, cf. (Doumiati et al., 2010a). That is, from the state-space model in (1), we impose, for consistency, that $B_2 M_z(t) = B_1 \delta_f(t)$. Then, using the pseudo-inverse matrix, we take $\delta_f = \left[(B_1^\top\ B_1)^{-1}\ B_1^\top\ B_2\right]\ M_z$. Since B_1 has full column rank [1] in (1), $(B_1^\top B_1)^{-1}$ is invertible. Accordingly, during the implementation of our H_∞ controller, we apply the following gain relation from its output (a fictional δ_f) to the real control input (yaw moment M_z):

$$M_z(t) = \left(-\frac{l_f\ m^2\ V_x^2(t)}{I_z^2\ c_f + c_f\ l_f^2\ m^2\ V_x^2(t)} \right)^{-1} \delta_f(t)\,. \quad (7)$$

Finally, using this input transformation, we stress that the frequency analysis of the synthesized controller demonstrates a positive gain margin, i.e. the closed-loop is stable. As indicates (Zhou and Doyle, 1998), a phase margin higher than 45 degrees indicates good stability robustness and a delay margin of 0.892 seconds suggests sufficient robustness to delays present in the real vehicle. Furthermore, regarding the performance and robustness of the proposed controller, we indicate that the optimisation problem in (3) yielded an optimal gain γ_∞ of 0.89, which represents a near-optimal result. Ideally, this gain should be closer to 1, but a compromise was made between performance, robustness and stability, limiting γ_∞ for optimality.

[1] In other words, the columns of B_1 must be linearly independent, guaranteeing that $(B_1^\top B_1)$ is invertible.

5. RESULTS

Considering the proposed robust lateral scheme for direct yaw moment control with the $\mathcal{H}_\infty$ loop and the LPV reference model, we present, next, numerical and experimental validation results to demonstrate the effectiveness of the method. To this end, we debate our proposition w.r.t. industrial (look-up table based) PID controllers - which are actually used in state-of-practice modern vehicles.

5.1 Numerics

First, we present a high-fidelity simulation result to demonstrate the stability and robustness of the proposed control scheme under parameter variations. For fidelity, we employ the full nonlinear dynamic vehicle model described in (Kissai, 2019). In particular, we test the proposed $\mathcal{H}_\infty$ controller via online computation using *Matlab*. Our simulations were performed on a computer equipped with an AMD Ryzen 3 processor, 8 GB of RAM, and a 256 GB SSD.

Accordingly, we qualitatively evaluate the robustness of the proposed lateral controller against a specific system uncertainty: mass variation. As illustrated in Fig. 6, we consider a road vehicle performing a"zig-zag" lateral manoeuvrer under a constant longitudinal velocity of $V_x = 90$ km/h, on a road with a friction coefficient $\mu = 1$.

The corresponding control signal (yaw moment) is presented in Fig. 5. Since the controller was synthesised using a "medium" mass value $m = m_M$, the control input M_z for a low mass $m = m_M - \delta m$ scenario has to compensate the uncertainty using a more aggressive policy, while for a high mass condition, the control becomes inverted since $m = m_M + \Delta m$. The resulting control strategy achieves the yaw rate regulation performance presented in Fig. 6.

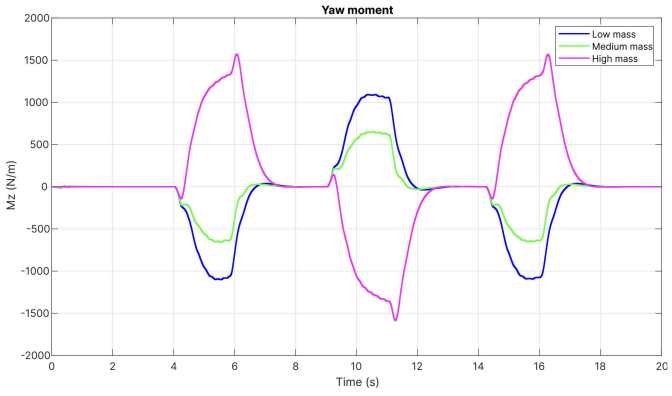

Fig. 5. Yaw moment - low, medium and high mass.

In Fig. 6, the reference trajectory (red line) is compared against the yaw rate responses for low (blue line), medium (green line, which corresponds to the mass parameter during the controller synthesis procedure), and high (pink line) vehicle masses. This numerical comparison serves to underscore our controller's consistent performance across varying mass configurations, demonstrating its robustness

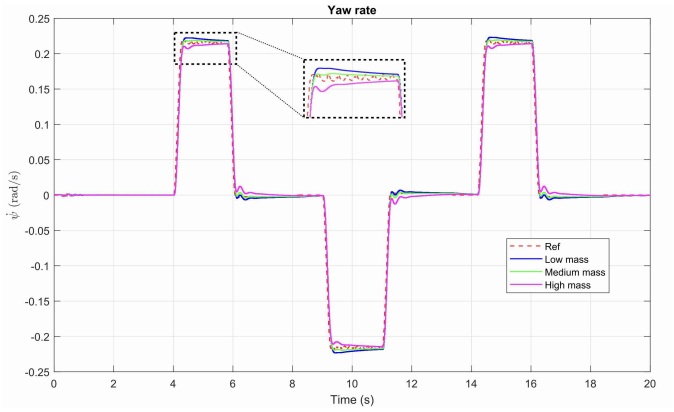

Fig. 6. Simulation for different mass.

in handling changes in vehicle dynamics with a single tuning. In contrast, we stress that the aforementioned industrial PID controller achieved comparable results in simulation, but required multiple tuning steps to accommodate the different yaw rate set-points - which highlights a significant advantage of the proposed approach with its embedded adaptive LPV reference model.

5.2 Experimental validation

The main contribution of this paper is the experimental validation of the LPV/$\mathcal{H}_\infty$ direct yaw moment control. To this end, two scenarios were tested in ascending order of control demand: to, respectively, evaluate control efficiency w.r.t. stability and handling performances during tests.

The prototype vehicle equipped with a MicroAutobox, an embedded PC platform capable of reading sensor data and sending signals to the vehicle's actuators. Then, in order to implement our robust control scheme within this environment, it was necessary to translate the Matlab/Simulink code (w.r.t. the numerical test) to C syntax and compile it into the MicroAutobox. Another necessary modification was the addition of a switch activation rule, in order to ensure that the controller would only be activated for longitudinal velocities greater than 30 km/h.

In experimental essays, a version of the control scheme without the reference model was also evaluated using the same weighting functions. This one exhibited an excessively strong control input and failed to maintain appropriate handling performances (as expected, from numerical simulation). These results highlight the fundamental importance of the reference model, which enables the controller to capture more precise representations of the real system dynamics and ensures stable performance.

During experimental tests shown subsequently, the prototype vehicle carried three people, i.e. the car ran under a medium mass configuration. Additionally, light rain occurred during the test day, which resulted in a slightly reduced road adhesion coefficient, providing a more challenging scenario for evaluation. The vehicle was also tested in "normal" and "sport" driving modes. Two experimental test conditions were tested: a "city" track and a "mountain" circuit.

City track: This first experimental track emulates an urban environment with typical "soft" curves and a roundabout. It was designed to represent standard city driving conditions and to test the stability of the proposed control scheme at low longitudinal speeds. Fig. 7 presents the GPS data from testing, where the red "x" sign marks the start point of the course.

Fig. 7. City track: The recorded trajectory.

In Fig. 8 we present the car's input signals: the steering wheel angle $\delta(t)$ and the vehicle's longitudinal velocity $V_x(t)$ (disturbances to the proposed control scheme). In particular, we stress that the latter remained below 50 km/h (i.e. low speed), and the steering angle averaged within the ± 200 degree range. Accordingly, these signals result in the yaw rate performance shown in Fig. 9.

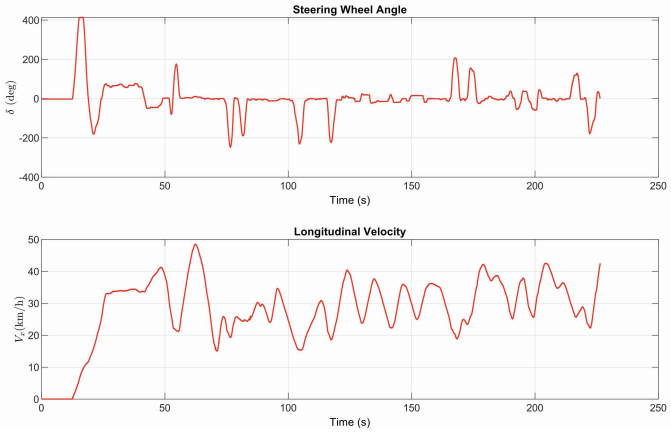

Fig. 8. City track: Pilot's inputs (disturbances).

As shown in Fig. 9, a somewhat less accurate tracking performance can be observed at the first peak. However, this is attributed to the transition between the control system being turned on for velocities greater than 30 km/h. Along the remainder of the driving scenario, the measured yaw rate (blue line) follows the reference trajectory generated by the LPV scheme very accurately, demonstrating effective performance of the proposed scheme. In particular, we emphasise that the corresponding Root Mean Square

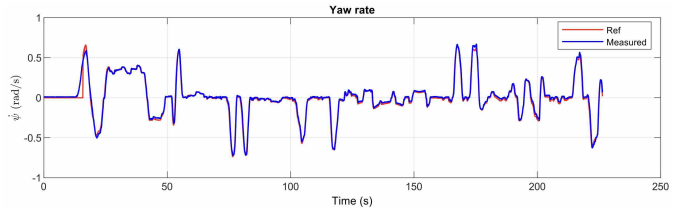

Fig. 9. City track: Yaw rate control for low speeds.

(RMS) index of the tracking error signal is very low, i.e. $\texttt{RMS}\left(\dot{\psi}(t) - \dot{\psi}_{\text{ref}}(t)\right) = 0.0366$. Moreover, we stress that the people inside the vehicle (particularly the test driver), during such city track, could clearly feel the proposed LPV/$\mathcal{H}_\infty$ system significantly assisting the lateral motion during the curves and manoeuvrers, thus enhancing handling (and stability).

Qualitatively [2], we indicate that the industrial (state-of-practice) PID scheme, driving along the same (city) course trajectory, leads to a yaw rate tracking with offset/bias in several points along the track. Furthermore, due to its dependency on the look-up table, the corresponding control results become entirely related to the quality and completeness of the "training" data used to populate the (PID gains) table. That is, the industrial PID is not able to ensure appropriate robustness due to the interpolation of data points. Our approach, however, is able to ensure robustness and appropriate tracking performance for all trajectory points.

Mountain circuit: Next, we present experimental results for a mountain circuit. This second track includes an ascending and descending road profile with tighter curves, similar to those found on a real mountain road. The track is significantly more demanding than the city track, and the corresponding tests enable the evaluation of the lateral control scheme performance w.r.t. handling.

In order to evaluate the proposed LPV/$\mathcal{H}_\infty$ control system's robustness under different setups, the car driving mode was set to "sport", resulting in more agile dynamics (i.e. with abrupt variations). As for the first track, the GPS data of this second course is given in Fig. 10.

As stated, the mountain circuit displayed in Fig. 10 comprises several slopes and narrow curves. Along this driving test, the vehicle's longitudinal velocity $V_x(t)$ exhibited an average close to 100 km/h, while the driver steering angle stayed within the ± 200 degree range (cf. Fig. 11). These (disturbance) signals generated the resulting yaw rate tracking performance presented in Fig. 12, which shows the reference signal and corresponding vehicle dynamic.

As in the first experimental test, Fig. 12 demonstrates that the proposed control system yields good tracking performances, even on the more challenging track - with a corresponding tracking RMS index of 0.0316. Qualitatively, we stress that the car pilot noted that the yaw moment control was aggressive, yet in a positive manner, helping him to maintain a good handling of the car during demanding curves. Correspondingly, in Fig. 13, the yaw

[2] Results using the PID scheme are industry-confidential and, thus, cannot be exhibited in this work.

Fig. 10. Mountain circuit: The recorded trajectory.

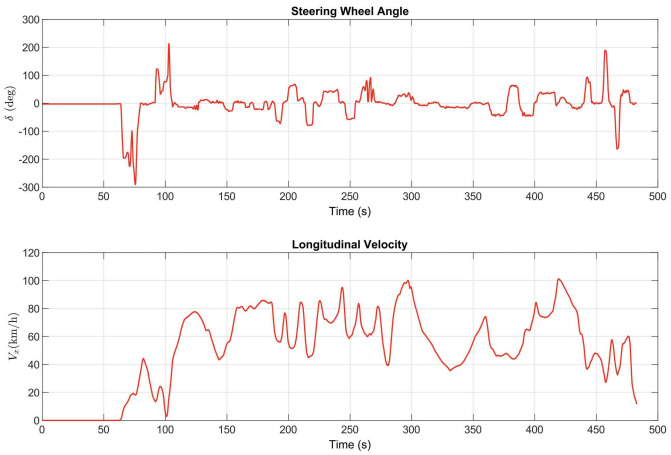

Fig. 11. Mountain circuit: Pilot's inputs (disturbances).

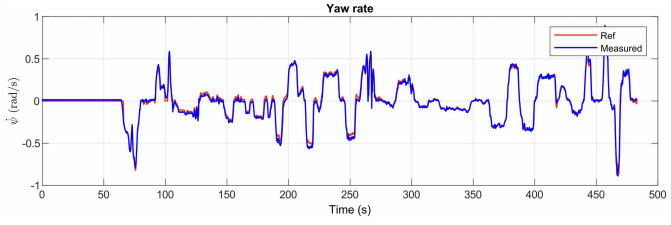

Fig. 12. Mountain circuit: Yaw rate control for high speed.

moment braking and rear steering angle are shown. Both these signals represent the outputs of the VMC scheme.

We highlight that following the experimental tests, the vehicle-embedded industrial PID controller was actually redesigned to match the frequency response of the proposed $\mathcal{H}_\infty$ controller. This adjustment was made given the propose scheme yaw rate tracking precision and its robustness to parameter variations (mass, road adhesion, etc) and system variables (transitions between "normal", "comfortable," and "sport" driving modes).

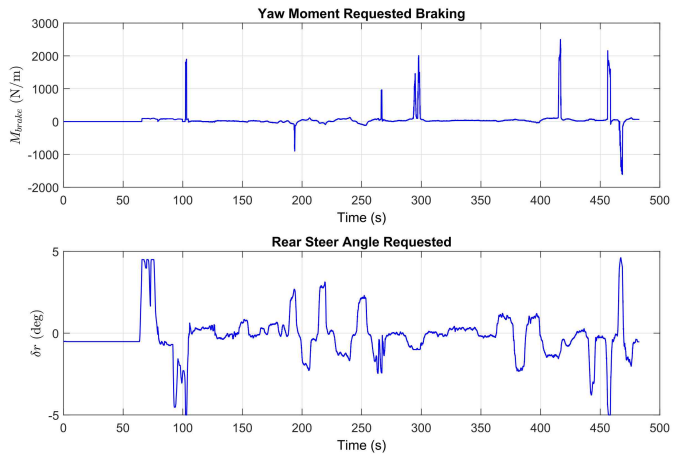

Fig. 13. Mountain circuit: Signals sent to the vehicle.

It is also worth noting that the $\mathcal{H}_\infty$ controller used in the presented experimental tests employed the same weighting functions as the one used in the simulation, which yielded promising results. Despite minor imperfections and implementation adjustments (w.r.t. the MicroAutobox), tuning the controller entirely in Matlab proved to be a fast and efficient method, unlike PID controllers that typically require extensive real-world testing for fine-tuning.

6. CONCLUSION AND OUTLOOK

This paper presented experimental validation results of a LPV/$\mathcal{H}_\infty$ scheme for direct yaw moment control, designed to enhance passenger comfort during sudden driving manoeuvrers. The controller was synthesized using an LPV reference model, the weighting functions were numerically determined and then validated with realistic simulations as well experimental tests. Our results demonstrate that the proposed controller performs effectively, even despite non-nominal model parameters (i.e. uncertainty), well handling variations in mass, road adhesion, and driving modes that directly impact the vehicle's dynamics.

In future works, we plan to implement a gain-scheduled LPV/$\mathcal{H}_\infty$ controller to further improve robustness, particularly under more challenging road conditions.

ACKNOWLEDGEMENTS

The Authors acknowledge the financial support from the Brazilian funding agencies CNPq [grants 304032/2019-0, 403949/2021-1, and 406477/2022-1] and CAPES [finance code 001 and grant 88881.878833/2023 – 01 - OPCOMPLEX, SticAmSud].

This work has been funded by European Union's Horizon Europe research and innovation programme under the *Marie Skłodowska-Curie Action* grant agreement No 101149263 (*REAL OPT 4 CONTROL*).

Funded by the European Union

REFERENCES

Aripin, M., Md Sam, Y., Danapalasingam, K.A., Peng, K., Hamzah, N., and Ismail, M. (2014). A review of active yaw control system for vehicle handling and stability enhancement. *International journal of vehicular technology*, 2014.

Doumiati, M., Sename, O., Martinez, J., Dugard, L., and Poussot-Vassal, C. (2010a). Gain-scheduled LPV/$\mathcal{H}_\infty$ controller based on direct yaw moment and active steering for vehicle handling improvements. In *49th IEEE Conference on Decision and Control (CDC)*, 6427–6432. doi:10.1109/CDC.2010.6171089.

Doumiati, M., Sename, O., Martinez, J., Dugard, L., and Poussot-Vassal, C. (2010b). Gain-scheduled LPV/$\mathcal{H}_\infty$ controller based on direct yaw moment and active steering for vehicle handling improvements. In *49th IEEE Conference on Decision and Control (CDC)*, 6427–6432. IEEE.

Hachem, M., Borrell, A.M., Sename, O., Atoui, H., and Morato, M. (2023). ROS implementation of planning and robust control strategies for autonomous vehicles. *Electronics*, 12(17), 3680.

Kiencke, U., Nielsen, L., Sutton, R., Schilling, K., Papageorgiou, M., and Asama, H. (2006). The impact of automatic control on recent developments in transportation and vehicle systems. *Annual reviews in control*, 30(1), 81–89.

Kissai, M. (2019). *Optimal Coordination of Chassis Systems for Vehicle Motion Control*. Theses, Université Paris Saclay (COmUE). URL `https://pastel.hal.science/tel-02292877`.

Lenzo, B., Zanchetta, M., Sorniotti, A., Gruber, P., and De Nijs, W. (2020). Yaw rate and sideslip angle control through single input single output direct yaw moment control. *IEEE Transactions on Control Systems Technology*, 29(1), 124–139.

Medero, A., Morato, M.M., Puig, V., and Sename, O. (2022). MPC-based optimal parameter scheduling of LPV controllers: Application to lateral ADAS control. In *2022 30th Mediterranean Conference on Control and Automation (MED)*, 951–956. IEEE.

Morato, M.M., Jungers, M., Normey-Rico, J.E., and Sename, O. (2022). A predictive fault tolerant control method for qLPV systems subject to input faults and constraints. *Journal of the Franklin Institute*, 359(16), 9129–9167.

Morato, M.M., Nguyen, M.Q., Sename, O., and Dugard, L. (2019). Design of a fast real-time LPV model predictive control system for semi-active suspension control of a full vehicle. *Journal of the Franklin Institute*, 356(3), 1196–1224.

Nahidi, A., Kasaiezadeh, A., Khosravani, S., Khajepour, A., Chen, S.K., and Litkouhi, B. (2017). Modular integrated longitudinal and lateral vehicle stability control for electric vehicles. *Mechatronics*, 44, 60–70.

Sename, O., Borrell, A.M., Morato, M.M., et al. (2024). On robust and predictive control approaches for linear parameter varying systems: Application to vehicle lateral control. *Foundations and Trends® in Systems and Control*, 11(4), 285–380.

Sename, O., Gaspar, P., and Bokor, J. (2013). *Robust control and linear parameter varying approaches: application to vehicle dynamics*, volume 437. Springer.

Zhao, C., Xiang, W., and Richardson, P. (2006). Vehicle lateral control and yaw stability control through differential braking. In *2006 IEEE international symposium on industrial electronics*, volume 1, 384–389. IEEE.

Zhou, K. and Doyle, J.C. (1998). *Essentials of robust control*, volume 104. Prentice hall Upper Saddle River, NJ.